Local order and structural transitions in amorphous metal-metalloid alloys

Thomas A. Weber and Frank H. Stillinger
AT&T Bell Laboratories, Murray Hill, New Jersey 07974
(Received 25 October 1984)

The $Ni_{80}P_{20}$ alloy system has been investigated in both liquid and amorphous solid forms using molecular-dynamics computer simulation. Atomic interactions were modeled by central pair potentials selected to represent roughly the atomic sizes and relative bond strengths. Self-diffusion constants and pair-correlation functions have been determined as a function of temperature. By means of a mass-weighted steepest descent on the potential-energy hypersurface, dynamical configurations at various temperatures have been mapped onto nearby potential-energy minima (stable atomic packings). This establishes that the liquid phase for the alloy has a temperature-independent inherent structure. Comparison with diffraction data on real Ni-P alloys suggests (and we verify) that improved molecular-dynamics modeling is possible.

I. INTRODUCTION

Materials science has several preparative methods at its disposal which frustrate the natural tendency of substances to crystallize at low temperature, producing instead amorphous solids. These techniques include splat quenching,[1] vapor condensation onto cold surfaces,[2] chemical deposition,[3] and electrodeposition from solution.[4] In particular, many binary alloys have thus been produced in an amorphous solid form. Several examples of these binaries whose properties have been experimentally studied are Pd-Si,[5] Au-Si,[6] Ag-Cu,[7] Ni-P,[7,8] Ni-B,[9] and Cu-Zr.[9]

Alloys containing both metals and metalloids (B, Si, P) present interesting characteristics that require explanation at the atomic level. The presence of metalloid atoms appears to disrupt short-range order of the type necessary for the formation of crystal nuclei. In part, this seems to be due to the small size of metalloid atoms compared with the metal atoms among which they are mixed. It is also related to the strong bonds that evidently form between neighboring metal-metalloid atom pairs,[7,8] with the result that pairs of metalloid atoms tend statistically to avoid each other.

A substantial body of experimental data has been published on the binary metal-metalloid systems in the amorphous solid state. This includes extensive thermodynamic studies,[10] as well as x-ray-diffraction analysis of short-range order,[7,11] for various composition ranges. Spurred on by this accumulating data, several attempts have been implemented to simulate the atomic-packing structures in several of these amorphous binary alloys.[8,12–14]

The primary goal of the present project has been to apply, apparently for the first time, the molecular-dynamics method of computer simulation to binary metal-metalloid systems. By doing so we have attempted to gain some quantitative insight into the types of atomic interactions necessary to describe these materials. We have also striven to develop somewhat unconventional theoretical probes and techniques to explain structures and kinetic properties.

The Ni-P system has been selected as the principal focus of our study. Its phase diagram[10] shows the presence of a deep eutectic for a composition of 19 at. % P, at 880 °C, in comparison with the pure Ni melting point 1425 °C. No doubt the existence of this deep eutectic is related to the relative ease with which amorphous Ni-P alloys with near-eutectic composition can be produced. In line with this observation, our molecular-dynamics simulation has utilized a system comprising 120 Ni atoms and 30 P atoms (conventional composition notation: $Ni_{80}P_{20}$).

The Ni-P system is also a particularly favorable candidate for simulation on account of Cargill's extensive x-ray studies[7] on many samples with varying compositions, produced both by chemical deposition and by electrodeposition. We also note that Dixmier *et al.*,[8] and Harris and Lewis,[13,14] have reported computer-constructed models for the Ni-P alloy and have compared the resulting structure factors with those from x-ray-diffraction experiments.

The present molecular-dynamics study has been confined to fixed overall density and composition. Although each dynamical run conserves energy, we are able to vary that energy (and thus the temperature) between runs. In this way it is possible to study structure and dynamics at various temperatures in the amorphous solid region, as well as the equilibrium liquid at considerably higher temperature. In principle, this approach also permits systematic study of cooling-rate effects in production of amorphous solids from the liquid, an option not available in the prior, purely constructive modeling.

During the course of some of our molecular-dynamics runs, atomic configurations were periodically mapped onto nearby potential-energy minima. This mapping is accomplished by a "quenching" procedure[15–24] which removes all kinetic energy and then continuously deforms the system's configuration via a mass-weighted steepest descent on the potential-energy hypersurface. The Newtonian dynamics is not perturbed by this process, which merely proceeds in parallel. We have found from our previous studies on single-component simple fluids[21–23] that this configurational mapping markedly

enhances structural features which are otherwise largely obscured by thermal motions. It has also revealed the existence of a temperature-independent inherent structure in the liquid phase at constant density; one of our secondary objectives in the present project has been to see if binary mixtures had a similar property.

In Sec. II we discuss our initial choice for pair potentials acting between metal and metalloid atoms. In this section we also outline the specifics of the molecular dynamics and of the periodically applied "quenching" procedure. In Sec. III we present global properties calculated for the system at various temperatures, including average potential energy, and separate diffusion constants for metal and metalloid atoms.

In Sec. IV we discuss characteristics of the potential-energy minima that were generated by the quenching (mapping) procedure. Especially noteworthy among these are the distribution of minima by depth, and the way their harmonic vibrational partition functions correlate with depth. In Sec. V we describe short-range order in the $Ni_{80}P_{20}$ system produced by our molecular-dynamics simulation, viewed both from the conventional pair-correlation function, as well as from those extracted from the corresponding sets of quenched configurations. Once again, we find that a temperature-independent inherent structure exists for the liquid phase. In Sec. VI we consider the transition states (saddle points on the potential-energy hypersurface) that connect neighboring minima, and provide evidence concerning localization of atomic motions along reaction coordinates that link those minima.

This paper ends with a discussion, Sec. VII, of how our initial choice of interactions might be modified to improve agreement with experiments on Ni-P alloys.

II. MODEL POTENTIAL AND SIMULATION PROTOCOL

In a recent series of molecular-dynamics computer studies,[18,20–24] we have found it convenient to represent pair interactions using the following family of functions:

$$v(r)=\begin{cases} A\,[(\alpha r)^{-p}-r^{-q}]\exp[(\alpha r-a)^{-1}], & 0<\alpha r\le a \\ 0, & \alpha r\ge a \end{cases} \tag{2.1}$$

where A, α, p, and a are all positive. The computational advantage of this form is that it has strictly limited range, but no discontinuities exist in the function itself or in any of its r derivatives. Sufficient flexibility is present to model substances which freeze into close-packed fcc crystals (such as the noble gases) or into bcc crystals (such as the alkali metals).

In the present study we have found it convenient to use reduced units which cause the metal-metal pair interaction to have unit depth, and to have a zero at $r=1$. The corresponding reduced potential energy then may be written

$$\Phi(\mathbf{r}_1,\ldots,\mathbf{r}_N)=\sum_{i<j}^{N} v_{\kappa(i)\kappa(j)}(r_{ij})\ , \tag{2.2}$$

where $\kappa(i)=$Ni,P indicates the species of atom i. The following choice of parameters applied to our simulation:

(a) For all interactions ($v_{\text{Ni-Ni}}$, $v_{\text{Ni-P}}$, $v_{\text{P-P}}$),

$$p=12,\quad q=0,\quad a=1.652\,194\ . \tag{2.3}$$

(b) For the metal-metal interaction ($v_{\text{Ni-Ni}}$),

$$A=8.805\,977,\quad \alpha=1.0\ . \tag{2.4}$$

(c) For the metal-metalloid interaction ($v_{\text{Ni-P}}$),

$$A=13.208\,965\,5,\quad \alpha=2.49/2.00=1.245\ . \tag{2.5}$$

(d) For the metalloid-metalloid interaction ($v_{\text{P-P}}$),

$$A=4.402\,988\,5,\quad \alpha=2.49/2.20=1.1318\ldots\ . \tag{2.6}$$

This choice yields the correct crystal structure (fcc) for the major constituent, Ni, in its pure form, and it produces bond lengths for pure Ni and pure P that have the proper ratio (2.49 vs 2.20 Å).[25]

Figure 1 shows plots of the three types of pair potential. It illustrates our working assumption that Ni-P pairs form the strongest, and thus the shortest, bonds. The relative depths are 1.0, 1.5, and 0.5 for Ni-Ni, Ni-P, and P-P pairs at the respective potential minima.

All of our molecular-dynamics simulations have involved 150 atoms, comprising 120 Ni's and 30 P's. These atoms were placed initially at random in a cube for which periodic boundary conditions applied. We have supposed that the atoms present were the stable isotopes, ^{62}Ni and ^{31}P, so that in our reduced units the masses could be tak-

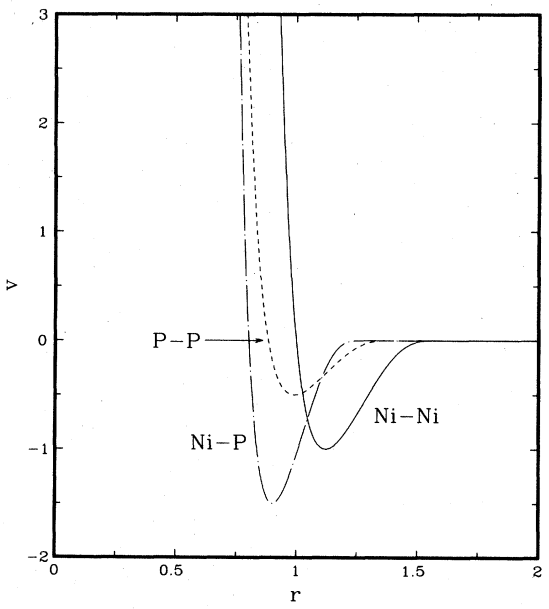

FIG. 1. Pair interaction potentials (in units of ε, the metal-metal interaction energy) as a function of interatomic separation distance (in units of σ, the metal-metal characteristic distance). Ni and P are the prototypical metal and metalloid atoms, respectively.

en, respectively, as 1.0 and 0.5.

The Newtonian equations of motion for the 150-atom system are

$$m_i(d^2\mathbf{r}_i/dt^2) = -\nabla_i\Phi \ , \tag{2.7}$$

where m_i is the mass of the ith atom. They were solved numerically using a fifth-order Gear algorithm[26] and reduced time increment $\Delta t = 5\times10^{-4}$. Classical dynamical trajectories of 10^4 time steps were generated to determine properties of the alloy at each temperature. Momentum scaling was used to vary system energy and thus the temperature; after each such scaling, relaxation runs of at least 2×10^3 time steps were interposed before calculating properties.

During the course of the molecular-dynamics simulation, instantaneous configurations of the 150 atoms were sampled (typically every 100 time steps) and subjected to a mass-weighted steepest-descent "quench" to locate the structurally relevant potential-energy minimum. The set of differential equations which determine this mapping onto minima is a first-order analog of the Newtonian dynamical equations, namely

$$m_i(d\mathbf{r}_i/ds) = -\nabla_i\Phi \ . \tag{2.8}$$

The inclusion of particle masses (unnecessary for the single-component cases considered before[18,21,23]) ensures concordance with the usual definition of reaction coordinates crossing potential-energy saddle points. The $s\to+\infty$ solutions to Eq. (2.8) were constructed using a combination of conjugate-gradient and Newton's methods.[27]

In order to compare results with measurements on real Ni-P alloys, it is necessary to redimension the dimensionless data which emerge from the molecular-dynamics simulation. We have already noted that the ^{62}Ni atom provides the mass unit:

$$m_{\mathrm{Ni}} = 1.0284\times10^{-22} \text{ g} \ . \tag{2.9}$$

Energy and length units, ε and σ, respectively, are introduced so that the redimensioned potential energy is

$$\varepsilon\,\Phi(\sigma\mathbf{r}_1, \ldots, \sigma\mathbf{r}_N) \ . \tag{2.10}$$

By choosing

$$\sigma = 2.2183 \text{ Å} \ , \tag{2.11}$$

the minimum in $v_{\mathrm{Ni\text{-}Ni}}$ occurs at the observed nearest-neighbor distance of the Ni, namely 2.49 Å. Furthermore, if

$$\varepsilon = 1.8546 \text{ kcal/mol} = 1.2879\times10^{-13} \text{ erg/atom} \ , \tag{2.12}$$

then the known reduced melting-point temperature (1.85) for the pure model system with $v_{\mathrm{Ni\text{-}Ni}}$ interactions[17] will agree with the measured melting temperature (1453 °C) for pure Ni. On this basis, the observed eutectic temperature (880 °C) corresponds to reduced temperature 1.2358.

The edge length L for the cubic box is

$$L = 5.3407\sigma = 11.8475 \text{ Å} \ . \tag{2.13}$$

With the 120 ^{62}Ni and 30 ^{31}P atoms in this volume, the mass density is 8.348 g/cm^3. Although experimentally prepared amorphous Ni-P alloys have lower mass densities in this composition range due to their different isotopic composition, our atomic-number density agrees with experiment.[7]

The fundamental time unit for these calculations is

$$\tau = \sigma(m_{\mathrm{Ni}}/\varepsilon)^{1/2} = 6.2721\times10^{-13} \text{ s} \ . \tag{2.14}$$

Consequently, each molecular-dynamics run of 10^4 time steps used for calculating averages spanned $5\tau = 3.1361$ ps.

III. GLOBAL PROPERTIES

Figure 2 shows a plot of average potential energy per atom, φ, as a function of temperature, T, both shown in reduced units. Each data point represents the mean value extracted from a dynamical trajectory of length 3.1361 ps. The points were generated both during heating and cooling stages of the study.

The scatter exhibited by the results at the low-temperature extreme ($T\approx0.2$) reflects the different thermal histories involved. Depending on cooling rate from high temperature and the vagaries of the specific trajectories executed in the 450-dimensional configuration space, the system can be trapped in any one of many regions surrounding potential minima. In any case, the sys-

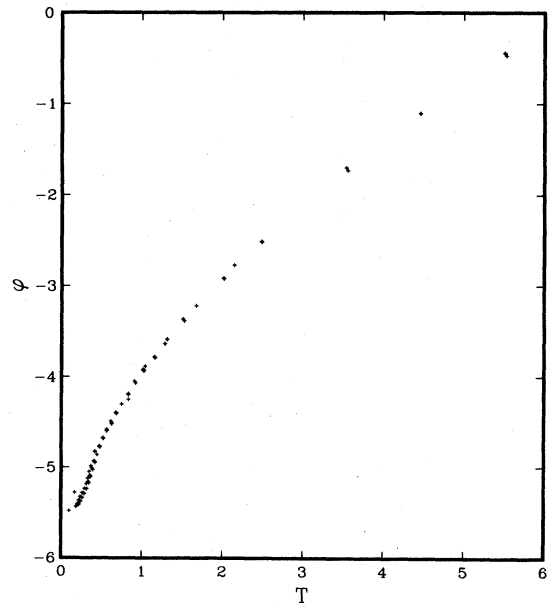

FIG. 2. Average potential energy per atom as a function of temperature in reduced units.

tem has consistently failed to discover crystalline minima. The low-temperature cases shown all correspond to rigid amorphous packings of the Ni and P atoms.

Mean-square displacements of the atoms of a given species κ=Ni,P asymptotically increase at a rate determined by the corresponding self-diffusion constant D_κ:

$$D_\kappa \sim \tfrac{1}{6}(d/dt)\langle\,|\,\mathbf{r}_i(t)-\mathbf{r}_i(0)\,|^2\rangle_\kappa\,. \tag{3.1}$$

We have evaluated D_{Ni} and D_{P} by this means, with the results shown in Fig. 3. Although some scatter is evident over the medium- to high-temperature range, two important features are clearly evident. First, the metalloid atoms diffuse faster than the metal atoms at all temperatures, as might have been expected due to their smaller size and mass. Second, the diffusion rate for both species drops dramatically to essentially zero when the reduced temperature declines below about 0.45. This is the same temperature region where the potential energy per atom shown in Fig. 1 changes most rapidly with temperature. Although the time scale of our simulation is necessarily very short by conventional experimental standards, it is still reasonable for this small system to identify this "transition region" as that leading to formation of a glasslike amorphous solid.

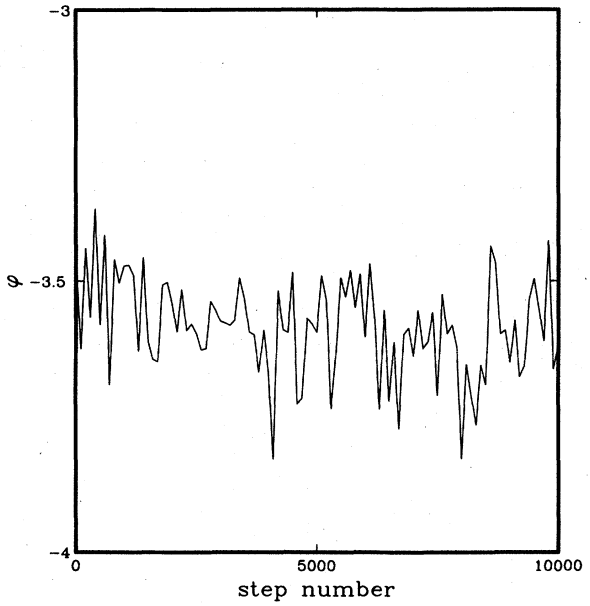

FIG. 4. Plot of potential energy per atom as a function of time step. The average temperature (in reduced units) for the run was $T=1.311$.

IV. POTENTIAL-ENERGY MINIMA

Figure 4 indicates time variation of potential energy per atom φ along a 10^4-time-step dynamical trajectory. The average kinetic energy along this trajectory corresponds to reduced temperature 1.311, slightly above the eutectic temperature. In principle, $\varphi(t)$ is continuous and differentiable for such a case; Fig. 4, however, consists of straight-line segments connecting discrete samplings taken every 100 time steps. This suffices to convey roughly the range and rate of fluctuations involved.

At each of the 101 sampling instants the system configuration was mapped onto the relevant potential-energy minimum by the mass-weighted steepest-descent procedure discussed above. The resulting values of the "quench" potential per atom appear in Fig. 5. It is obvi-

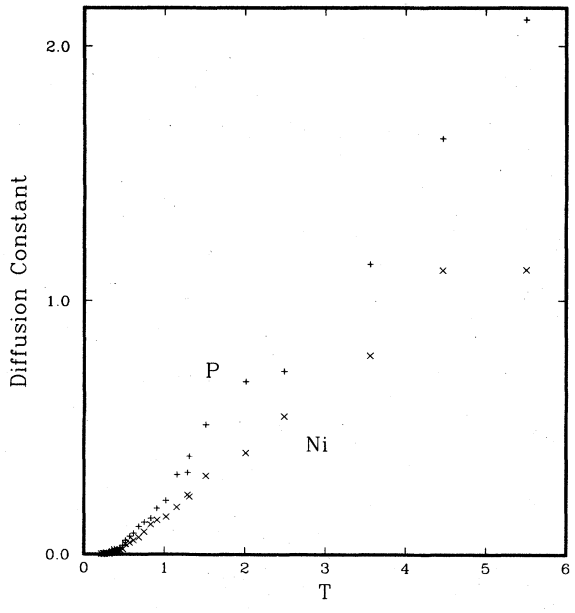

FIG. 3. Diffusion constants (in units of 10^{-7} cm^2/sec) vs temperature (reduced units). The pluses mark the metalloid data. The ×'s mark the metal data.

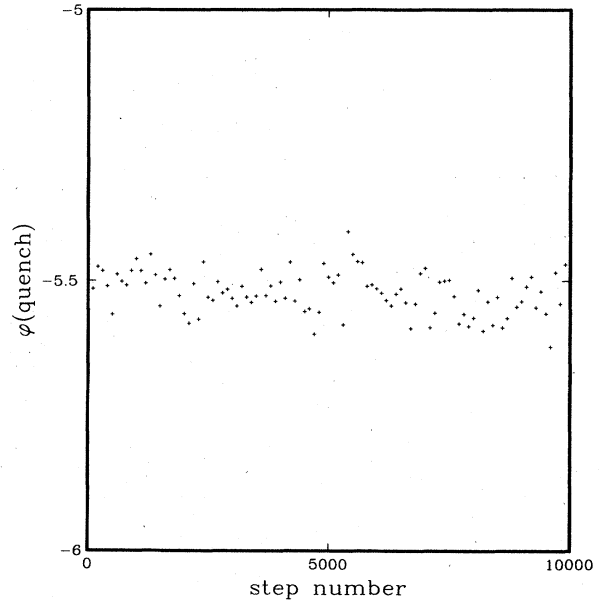

FIG. 5. Plot of potential energy per atom of the quenched configurations as a function of time step. The average prequench temperature was $T=1.311$.

ous that these must all be more negative than the corresponding initial φ values along the dynamical trajectory. Less obvious is the conclusion that the minima encountered upon quenching fluctuate considerably less in depth than do the initial $\varphi(t)$ values.

Substantially the same distribution (in depth) of potential-energy minima has been observed when the mapping procedure was carried out in the same fashion, but from trajectories at the higher reduced temperatures of 1.67, 5.50, 7.38, and 24.93. Consequently, all five cases were combined to produce the histogram shown in Fig. 6. We believe that this constitutes a reasonably good determination of the *a priori* distribution, by depth, of all potential-energy minima available to our $Ni_{80}P_{20}$ system.

The distribution in Fig. 6 appears to be unimodal and substantially symmetrical. This pattern differs from those previously observed for single-component systems that could readily crystallize,[18,24] where, instead, the distributions tend to be skewed markedly in the negative-φ direction. Furthermore, those crystallizable cases, at the most negative extreme, show nonmonotonic "banding" that is associated with crystal defects in varying numbers.

The character of packing structures for the potential minima, and local environment of atoms in those packings, may be probed by the vibrational normal modes at the minima. The corresponding classical vibrational partition function (in that harmonic approximation) has the following product form:

$$Z_{\rm vib}^{(0)}=\prod_l (\beta\hbar\omega_l)^{-1} , \tag{4.1}$$

where $\beta=(k_B T)^{-1}$, and ω_l is the angular frequency for mode l. In the present circumstance with periodic boundary conditions, there are $3N-3$ positive frequencies, and the product in Eq. (4.1) is restricted just to those.

The spectrum of normal modes varies from one Φ minimum to the next in a manner which can be examined numerically with no great difficulty for our 150-atom system. The angular frequencies ω_l are determined by the eigenvalues of the secular equation

$$|\boldsymbol{K}-\omega^2\boldsymbol{I}|=0 , \tag{4.2}$$

where $\boldsymbol{I}$ is the unit matrix. The elements of $\boldsymbol{K}$ are given by

$$K_{i\alpha,j\gamma}=(m_i m_j)^{-1/2}(\partial^2\Phi/\partial x_{i\alpha}\partial x_{j\gamma}) , \tag{4.3}$$

where $x_{i\alpha}$ denotes the αth component of the position vector $\mathbf{r}_i$ for atom i and where the derivative indicated is to be evaluated at the minimum of interest.

The nontrivial part of the harmonic vibrational free energy is given by the quantity

$$\sum_j \ln\omega_j=-\ln[(\beta\hbar)^{3N-3}Z_{\rm vib}^{(0)}] . \tag{4.4}$$

Figure 7 provides a correlation diagram for many examples of this quantity plotted against the respective Φ values at those minima. These data were extracted from selected molecular-dynamics runs that span virtually the entire temperature range covered in this study.

Although Fig. 7 displays considerable scatter, it also reveals obvious statistical correlation: Large values of $\sum \ln\omega_j$ tend to be associated with the most negative Φ's. In other words, the deepest minima tend to be vibrationally the stiffest. This kind of correlation has been recog-

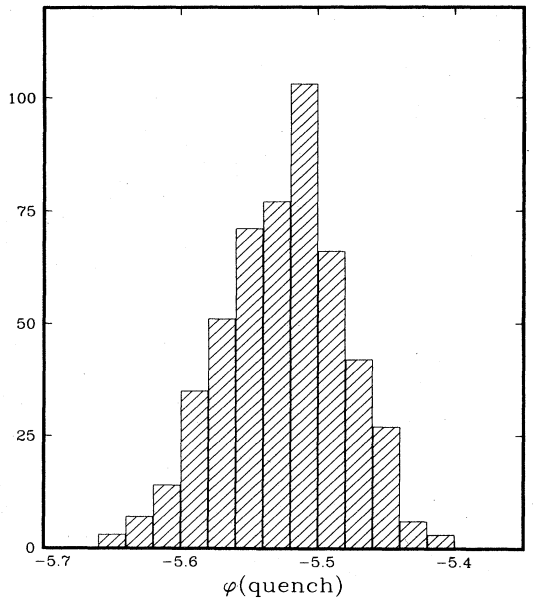

FIG. 6. Plot of the distribution of the energies of the quench configurations.

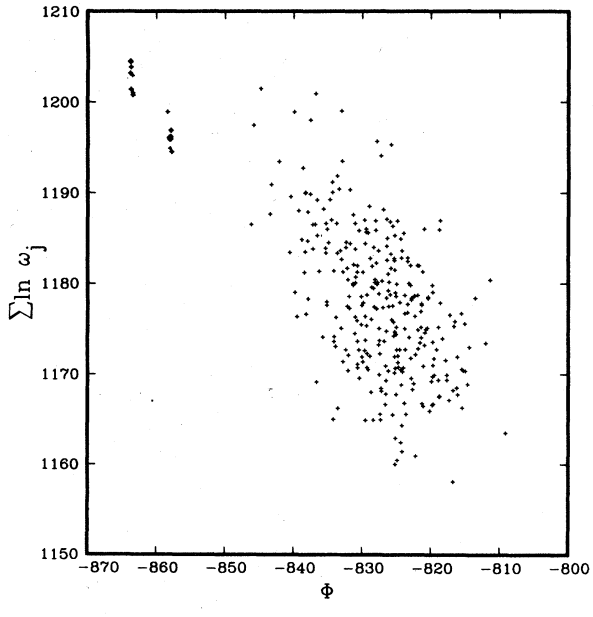

FIG. 7. Plot of $\sum_j \ln\omega_j$ vs the total potential energy for quench configurations.

nized before in models for single-component systems that can crystallize.[24] It should be pointed out that the two clusters of states in the upper left-hand corner of Fig. 7 emerged from two runs carried out at very low reduced temperatures (0.1862 and 0.2217).

V. PAIR-CORRELATION FUNCTIONS

Three radial pair-correlation functions $g_{\text{Ni-Ni}}$, $g_{\text{Ni-P}}$, and $g_{\text{P-P}}$ convey basic geometric information about atom arrangements in the Ni-P system. These are defined by the requirement that two volume elements, dV_1 and dV_2, separated by distance R_{12}, will, respectively, be occupied by species μ and κ (Ni or P) with probability

$$\rho_\mu \rho_\kappa g_{\mu\kappa}(R_{12}) dV_1 \, dV_2 \ , \tag{5.1}$$

where the number densities have been denoted by ρ_μ and ρ_κ, and where averaging over directions is implicit. In an infinite system the normalization imposed by Eq. (5.1) causes the $g_{\mu\kappa}$ to approach 1 at large R_{12}.

Figures 8—10 present examples of these three pair-correlation functions from the molecular-dynamics simulation. Each figure contrasts one of the $g_{\mu\kappa}$ (with vertical offset) evaluated at two reduced temperatures, namely 1.31 and 24.93. Using the redimensioning scheme discussed earlier, these reduced temperatures convert, respectively, to 928 °C and 22 990 °C. The former is only slightly above the eutectic temperature (880 °C) and well within reasonable experimental limits. Obviously, the latter is outside of the experimental regime, but we find it, theoretically, to be an illuminating extreme case to include, and, in fact, it was the highest temperature examined in our constant-density simulation.

The curves in Figs. 8—10 show, as expected, that raising the temperature diminishes the magnitude of short-range order. It should be remarked that we have also examined intermediate-temperature cases and find results that interpolate simply between those shown. Not only does higher temperature cause amplitude reduction in correlation peaks and valleys, but it also permits a greater extent of repulsive core interpenetration, as revealed, for example, by the inward shift of the first peak.

The results presented in Fig. 10 for $g_{\text{P-P}}$ are rather

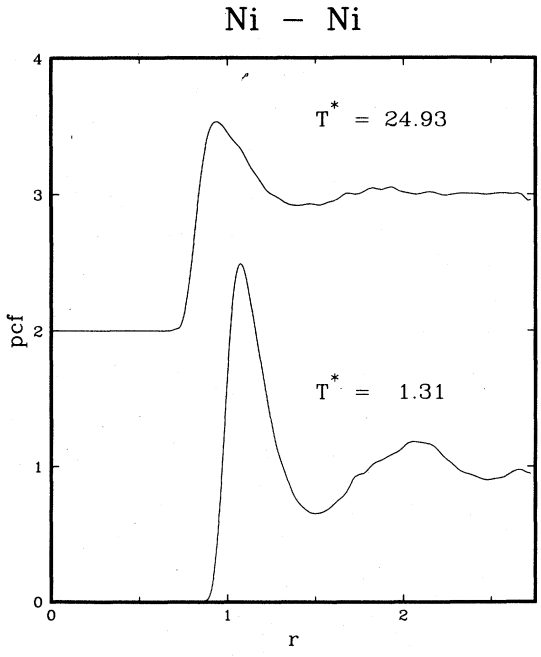

FIG. 8. Metal-metal pair-correlation functions. The zero of the high-temperature case has been offset.

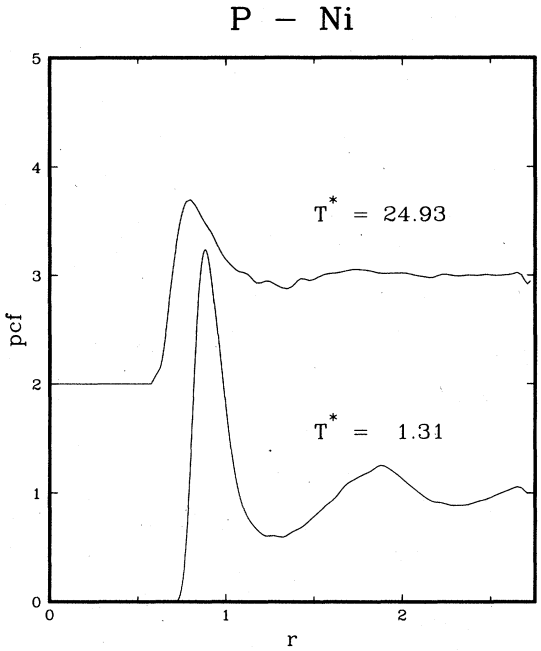

FIG. 9. Metal-metalloid pair-correlation functions.

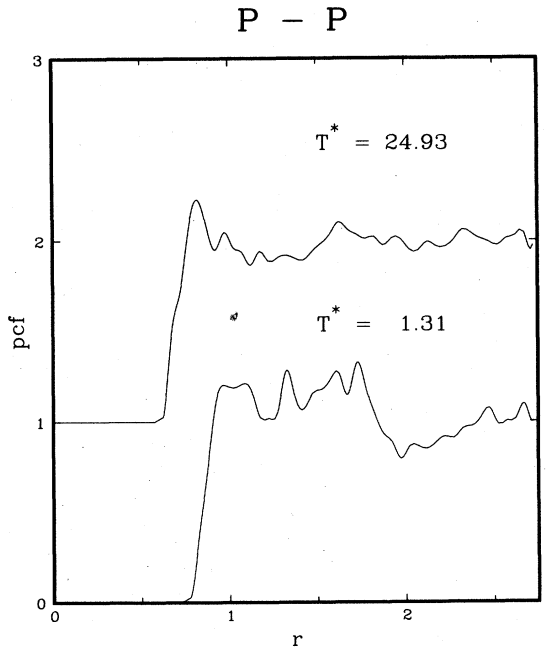

FIG. 10. Metalloid-metalloid pair-correlation functions.

noisy due to the smaller number of atom pairs of this type, compared with the other two types. However, it is clear that, aside from a very small distance exclusion, the P-P pairs are largely uncorrelated, even at the lower temperature. This contrasts sharply with the substantial short-range order displayed for Ni-Ni and Ni-P pairs.

We have also calculated "quench" pair-correlation functions $g_{\mu\kappa,q}$ for the two thermodynamic states represented in Figs. 8—10. These were obtained from the configurations at potential minima resulting from the mapping procedure discussed above. For both initial temperatures, 101 mappings, equally spaced in time by 0.031 361 ps along the initial trajectory, were created for this purpose. In Figs. 11—13 we present the results.

It is immediately obvious by comparing Figs. 11—13, respectively, with Figs. 8—10, that the mapping produces a significant "image enhancement" with respect to short-range order present in the system. Evidently, the thermally excited vibrational displacements away from potential minima obscure the perception of short-range order present in this condensed-matter system.

The pairs of $g_{\mu\kappa,q}$ results in Figs. 11—13 stemmed from widely different temperatures, yet these pairs are virtually superimposable, with any discrepancy of the order of expected statistical error for our finite sampling. We find essentially identical results at intermediate temperatures. This observation verifies the existence of a temperature-independent inherent structure for the thermodynamically stable liquid region of the Ni-P system, and thus extends similar observations we previously made for single-component models.[21,23]

We expect that the temperature-independent inherent structure must eventually become irrelevant as the system is cooled into the very-low-temperature glassy regime. In that case, the results both before and after mapping would reflect essential nonergodicity of trapping into special phase-space regions, and would be explicitly dependent on cooling history.

On account of the remarkable structural enhancement

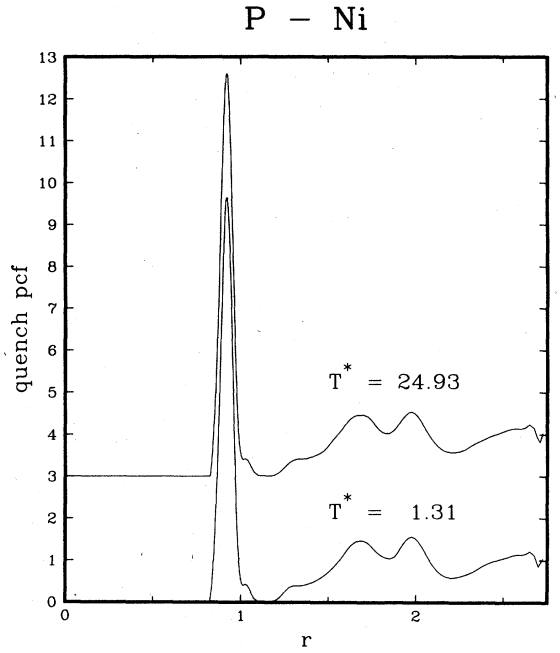

FIG. 12. Metal-metalloid pair-correlation functions determined from the quenched configurations.

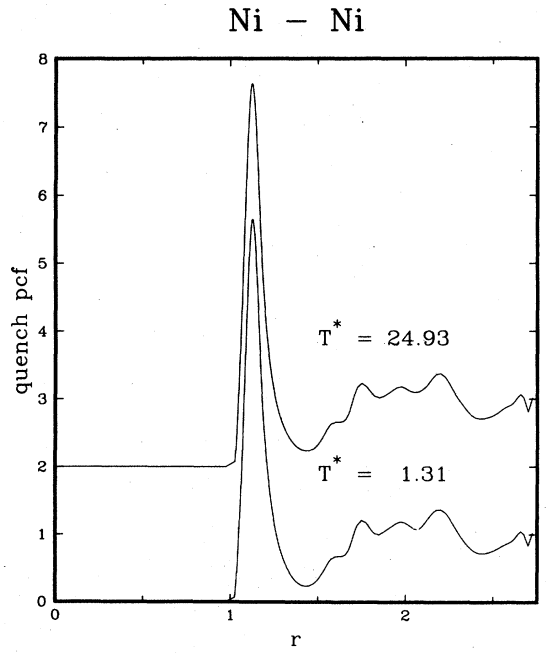

FIG. 11. Metal-metal pair-correlation functions determined from the quenched configurations.

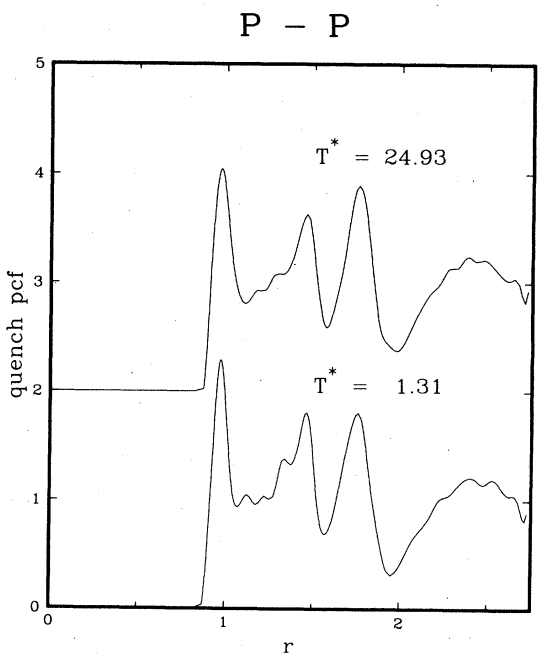

FIG. 13. Metalloid-metalloid pair-correlation functions determined from the quenched configurations.

produced by mapping to minima, interpretation is simplified. Note, in particular, that assigning a mean coordination number for P's by Ni's on the basis of conventional radial pair-correlation functions ($g_{\text{Ni-P}}$ in Fig. 9) is somewhat equivocal due to the breadth and shallowness of the minimum beyond the first peak, and this is especially vexing at high temperature. However, the common "quench" function in Fig. 12 resolves this difficulty fully because $g_{\text{Ni-P},q}$ is identically zero over a small range, and leads to an unambiguous mean coordination number of 7.1 Ni's around each P.

VI. FUNDAMENTAL TRANSITIONS

As the dynamical trajectory in phase space takes the system forward in time, it visits a sequence of regions each of which is associated with a potential minimum by the mapping. If the total system energy is low, the transitions between successively visited regions can be expected to pass near simple saddle points, "transition states" in the parlance of chemical-rate theory. It is valuable to study these saddle points and the associated barrier-crossing "reaction coordinates" to gain insight into relaxation processes.

Each simple saddle point (as well as each minimum) is an extremum of Φ satisfying

$$\Psi \equiv (\nabla\Phi)^2 = 0 \ . \tag{6.1}$$

Using this basic property, we previously utilized an heuristic procedure[24] to locate saddle-point configurations. This procedure begins by identifying two Φ-minimum configurations, say A and B, whose mapping regions are successively visited by a dynamical trajectory. Then Φ is evaluated along a linear path in the multidimensional configurational space between points A and B. Next, starting from the point of maximal Φ along this path (as a rough estimate of the saddle-point position), a steepest descent on the Ψ hypersurface is (approximately) followed until Eq. (6.1) is satisfied. The matrix of second Φ derivatives at the endpoint is then diagonalized to verify that one and only one negative eigenvalue exists there, corresponding to the reaction coordinate. The direction of the reaction coordinate can also be identified by initiating a Φ-hypersurface steepest descent from the simple saddle point.

It is important to determine the extent to which the fundamental transitions involve strictly localized rearrangements of just a small subset of the atoms, or whether the entire system typically transforms its packing geometry in such a transition. One way to clarify this issue is to examine the collection of three-dimensional displacement vectors

$$\mathbf{u}_i = \mathbf{r}_i^{(A)} - \mathbf{r}_i^{(B)} - \mathbf{s} \ , \tag{6.2}$$

which relate the coordinates of each atom i in the two minima. In this expression, $\mathbf{s}$ is a translation vector that brings the centroids of A and B into coincidence. The distributions of the $\mathbf{u}_i$'s can separately be examined for the Ni and P atoms for any given transition. If a global geometry change were involved for the entire system, it is reasonable to assume that (roughly) a three-dimensional Gaussian distribution of displacements would obtain, and in that event, for either species,

$$\langle\,|\mathbf{u}_i|^4\rangle_\kappa / (\langle\,|\mathbf{u}_i|^2\rangle_\kappa)^2 = 5/3 \ . \tag{6.3}$$

In contrast, transitions localized on a small set of atoms would have distinctly higher values of this characteristic moment ratio.

We find that the fundamental transitions are substantially more localized than would be represented by Gaussian distributions. A specific example suffices to illustrate this point, involving a fundamental transition during molecular dynamics at reduced temperature 0.186. The initial (A), final (B), and transition-state or saddle-point (ts) values of the potential were

$$\begin{aligned} \Phi^{(A)} &= -858.172\,126 \ , \\ \Phi^{(B)} &= -858.370\,557 \ , \\ \Phi^{(ts)} &= -858.144\,859 \ . \end{aligned} \tag{6.4}$$

Displacement averages for the 30 P atoms for this transition are

$$\begin{aligned} \langle u^2\rangle_{\text{P}} &= 0.001\,535\sigma^2 \ , \\ \langle u^4\rangle_{\text{P}} &= 0.000\,026\,56\sigma^4 \ , \\ \langle u^4\rangle_{\text{P}} / (\langle u^2\rangle_{\text{P}})^2 &= 11.273 \ . \end{aligned} \tag{6.5}$$

The corresponding results for Ni are

$$\begin{aligned} \langle u^2\rangle_{\text{Ni}} &= 0.001\,325\sigma^2 \ , \\ \langle u^4\rangle_{\text{Ni}} &= 0.000\,013\,44\sigma^4 \ , \\ \langle u^4\rangle_{\text{Ni}} / (\langle u^2\rangle_{\text{Ni}})^2 &= 7.663 \ . \end{aligned} \tag{6.6}$$

This localization (compared to the Gaussian case) qualitatively applies at all temperatures, but tends to be most obvious in the low-temperature limit.

We note that transition localization appears to be quite general, having, in fact, been previously observed in single-component models.[18] We have also found that the present binary mixture shares another attribute with the single-component case, namely that fundamental transitions are very rare between regions surrounding minima that differ only by permutation of identical particles.

VII. DISCUSSION

Each region in configuration space whose points map onto a common Φ minimum has a size and shape that depends on atomic-mass ratios. This arises through the mass weighting in the steepest-descent equations (2.7). At first sight, it would then seem that the inherent structure that we have identified for the binary Ni-P liquid ought to be mass dependent. In fact, this appears not to be the case. To test this point we reversed the mass ratio, so that P's temporarily were twice as massive as the Ni's. The conventional pair-correlation functions, of course, were unchanged by this switch (no mass dependence of equilibrium properties in classical statistical mechanics), but, likewise, the "quench" pair-correlation functions were unchanged within statistical error. Evidently, inherent

structure as defined in this paper is insensitive to the details of the mapping operation's mass weighting.

Admittedly, the atomic pair potentials used in our simulations were only a rough first estimate of the true interactions operative in real Ni-P alloys. Comparing our predictions for short-range order with that actually observed provides the opportunity to refine that first estimate.

Cargill[7] has measured the x-ray interference function $I(k)$ for amorphous Ni-P deposits in the composition range 73.8—81.4 at. % Ni, thus spanning the case examined here. The interference function is given by the Fourier transform of the radial density function $\rho(r)$:

$$I(k)=1+(4\pi/k)\int_0^\infty [\rho(r)-\rho_0]r\sin(kr)dr\ . \tag{7.1}$$

The radial density function is given by the expression

$$\begin{aligned}\rho(r)=\rho_0[\ & C_{\mathrm{Ni}}^2(f_{\mathrm{Ni}}^2/\langle f\rangle^2)g_{\mathrm{Ni\text{-}Ni}}(r)\\ &+2C_{\mathrm{Ni}}C_{\mathrm{P}}(f_{\mathrm{Ni}}f_{\mathrm{P}}/\langle f\rangle^2)g_{\mathrm{Ni\text{-}P}}(r)\\ &+C_{\mathrm{P}}^2(f_{\mathrm{P}}^2/\langle f\rangle^2)g_{\mathrm{P\text{-}P}}(r)]\ ,\end{aligned} \tag{7.2}$$

where the C_κ's are atomic mole fractions, ρ_0 is the average atomic-number density, and

$$\langle f\rangle^2=(C_{\mathrm{Ni}}f_{\mathrm{Ni}}+C_{\mathrm{P}}f_{\mathrm{P}})^2\ . \tag{7.3}$$

Following Cargill, we can assume that the atomic scattering factors f_κ are independent of k, and that

$$\begin{aligned}&C_{\mathrm{Ni}}f_{\mathrm{Ni}}^2/\langle f\rangle^2=1.00\ ,\\ &2C_{\mathrm{Ni}}f_{\mathrm{Ni}}f_{\mathrm{P}}/\langle f\rangle^2=0.93\ ,\\ &C_{\mathrm{P}}f_{\mathrm{P}}^2/\langle f\rangle^2=0.055\ .\end{aligned} \tag{7.4}$$

Hence we can proceed to calculate $I(k)$ using the molecular-dynamics pair-correlation functions $g_{\mu\kappa}(r)$.

Curve (a) in Fig. 14 shows the x-ray interference function for our model $Ni_{80}P_{20}$ alloy in its amorphous solid form near 300 K, which may be directly compared with Cargill's experiments. The shape of the curve for $k\sigma<5$ is artifactual due to finite-system truncation errors, and should be disregarded in this range. It should be noted, however, that in the significant range, the second peak near $k\sigma=12$ does not contain the prominent shoulder that is so evident in its experimental counterpart.

Figure 15, curve (a), shows the radial distribution function

$$rdf(r)=4\pi r^2\rho(r)/\rho_0 \tag{7.5}$$

for the same simulation run at approximately 300 K. The existence of the first small peak and the relative separation of the broad peaks around $r=2$ also do not agree with experimental findings. While our initial choice of interactions serves as a useful prototype, it obviously requires modification.

We have tested a modified interaction with encouraging results. Referring to Fig. 1, we simply increased the length scale of $v_{\mathrm{Ni\text{-}P}}$ to coincide with that of $v_{\mathrm{P\text{-}P}}$, i.e., we set $\alpha=2.49/2.20$ for the metal-metalloid pair potential. All other attributes of the interactions remained unal-

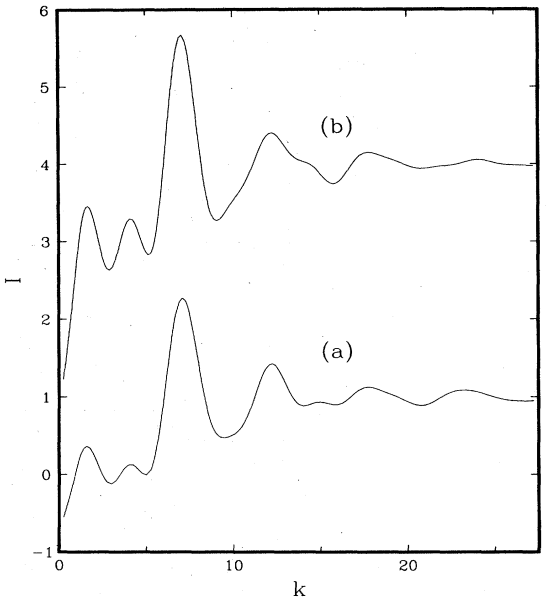

FIG. 14. X-ray scattering function of the metal-metalloid alloy near 300 K. Curve (a) is calculated with interaction potential given by Eqs. (2.1) and (2.2). Curve (b) is calculated with a modified interaction potential given by Eqs. (2.1) and (2.2) where the metal-metalloid interaction parameter has been changed to $\alpha=2.49/2.20$.

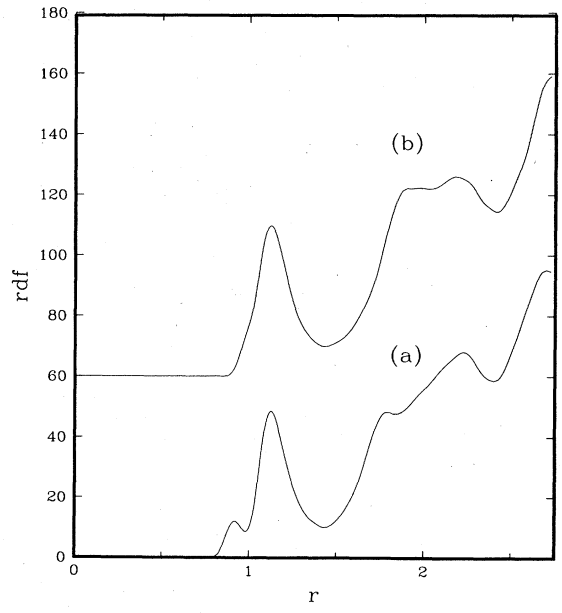

FIG. 15. Radial distribution functions [Eq. (7.5)] of the metal-metalloid alloy near 300 K calculated from the interference functions of Fig. 14.

tered, including relative depths.

Curves (b) in Figs. 14 and 15 show comparative results for 300 K that arise from this conservative modification. The new interference function and radial distribution function now agree far better with Cargill's experimental measurements. This is especially striking since the differences between the simulated and measured radial distribution functions are within differences noted by Cargill for amorphous deposits produced alternatively by chemical deposition or by electrodeposition.[7]

We do not believe that the bulk of the qualitative conclusions reached for the initial version of the interactions would be changed by the modification introduced for $\nu_{\text{Ni-P}}$. Specifically, a temperature-independent inherent structure (albeit a somewhat different one) should continue to exist for the liquid. Likewise, we expect an essentially symmetrical distribution (as in Fig. 6) of minima by depth, and a normal-mode—depth correlation (Fig. 7) to survive the modification. However, these matters are subject to later precise verification.

In applying our technique previously to low-temperature amorphous materials, we have occasionally observed localized bistable ("two-level") structures.[18] Harris and Lewis[13] have suggested that these states exist in amorphous alloys in concentrations that decline with the degree of annealing to which the sample has been subjected. Although we have not specifically focused on this feature in the present binary-alloy simulation, it is possible to identify and characterize collective bistable degrees of freedom in great detail, determining, for instance, how many atoms of each type move, by how much, and what the potential-energy variation is along the reaction coordinate. This is a subject to which we shall return in future studies of amorphous alloys.

[1]P. Duwez and R. H. Willens, Trans. Metall. Soc. AIME **227**, 362 (1963).

[2]S. Mader, J. Vac. Sci. Technol. **2**, 35 (1965).

[3]A. Brenner and G. Riddell, J. Res. Natl. Bur. Stand. **39**, 385 (1947).

[4]A. Brenner, D. E. Couch, and E. K. Williams, J. Res. Natl. Bur. Stand. **44**, 109 (1950).

[5]R. C. Crewdson, Ph.D. thesis, California Institute of Technology, Pasadena, 1966.

[6]J. Dixmier and A. Guinier, Rev. Metall. (Paris) **64**, 53 (1967).

[7]G. S. Cargill III, J. Appl. Phys. **41**, 12 (1970).

[8]J. Dixmier, K. Doi, and A. Guinier, in *Physics of Non-Crystalline Solids,* edited by J. A. Prins (North-Holland, Amsterdam, 1965), p. 67.

[9]E. Nassif, P. Lamparter, B. Sedelmeyer, and S. Steeb, Z. Naturforsch. **38a**, 1098 (1983).

[10]*Constitution of Binary Alloys,* 2nd ed., edited by M. Hansen and K. Anderko (McGraw-Hill, New York, 1958).

[11]G. S. Cargill III, in *Solid State Physics,* edited by H. Ehrenreich, F. Seitz, and D. Turnbull (Academic, New York, 1975), Vol. 30, p. 227.

[12]D. Weaire, M. F. Ashby, J. Logan, and M. J. Weins, Acta Metall. **19**, 779 (1971).

[13]R. Harris and L. J. Lewis, Phys. Rev. B **25**, 4997 (1982).

[14]R. Harris and L. J. Lewis, J. Phys. F **13**, 1359 (1983).

[15]F. H. Stillinger and T. A. Weber, Kinam **3A**, 159 (1981).

[16]F. H. Stillinger and T. A. Weber, Phys. Rev. A **25**, 978 (1982).

[17]F. H. Stillinger and T. A. Weber, J. Phys. Chem. **87**, 2833 (1983).

[18]F. H. Stillinger and T. A. Weber, Phys. Rev. A **28**, 2408 (1983).

[19]T. A. Weber and F. H. Stillinger, J. Chem. Phys. **80**, 438 (1984).

[20]T. A. Weber and F. H. Stillinger, J. Chem. Phys. **80**, 2742 (1984).

[21]F. H. Stillinger and T. A. Weber, J. Chem. Phys. **80**, 4434 (1984).

[22]F. H. Stillinger and T. A. Weber, Science **225**, 983 (1984).

[23]T. A. Weber and F. H. Stillinger, J. Chem. Phys. **81**, 5089 (1984).

[24]F. H. Stillinger and T. A. Weber, J. Chem. Phys. **81**, 5095 (1984).

[25]J. Donohue, *Structures of the Elements* (Wiley, New York, 1974).

[26]C. W. Gear, Argonne National Laboratory Report No. ANL-7126, Jan. 1966 (unpublished).

[27]R. Fletcher, *Practical Methods of Optimization* (Wiley, New York, 1980).